

Quantum paraelectric state and critical behavior in $\text{Sn}(\text{Pb})_2\text{P}_2\text{S}(\text{Se})_6$ ferroelectrics

I. Zamaraitė,¹ V. Liubachko,^{2,3} R. Yevych,² A. Oleaga,³ A. Salazar,³ A. Dziaugys,¹ J. Banys,¹ and Yu. Vysochanskii²

¹*Faculty of Physics, Vilnius University, Sauletekio 9, 10222 Vilnius, Lithuania*

²*Institute for Solid State Physics and Chemistry,*

Uzhhorod University, Pidgirna Str. 46, Uzhhorod, 88000, Ukraine

³*Departamento de Física Aplicada I, Escuela de Ingeniería de Bilbao, Universidad del País Vasco UPV/EHU, Plaza Torres Quevedo 1, 48013 Bilbao, Spain*

(Dated: March 24, 2020)

The dipole ordering in $\text{Sn}(\text{Pb})_2\text{P}_2\text{S}(\text{Se})_6$ materials may be tuned by chemical substitution realizing a ferroelectric quantum phase transition and quantum glassy or relaxor type phenomena on different parts of the phase diagram. The introduction of Ge impurity increases the temperature of the phase transitions and initiates a more pronounced Ising type critical anomaly in $\text{Sn}_2\text{P}_2\text{S}_6$ crystal, does not shift the coordinate of the Lifshitz point x_{LP} in $\text{Sn}_2\text{P}_2(\text{Se}_x\text{S}_{1-x})_6$ mixed crystals, induces the appearance of a ferroelectric phase transition in quantum paraelectrics $\text{Pb}_2\text{P}_2\text{S}_6$ and inhomogeneous polar ordering in $(\text{Pb}_{0.7}\text{Sn}_{0.3})_2\text{P}_2\text{S}(\text{Se})_6$ crystals. For $\text{Pb}_2\text{P}_2\text{S}_6$ crystal, the real part of the dielectric susceptibility in the quantum critical regime varies as $1/T^2$ instead of the expected $1/T^3$ behavior for uniaxial materials. This can be partially explained by a screening phenomenon in the semiconductor materials of the $\text{Sn}(\text{Pb})_2\text{P}_2\text{S}(\text{Se})_6$ system, which weakens the long range electric dipole interactions, and also provides, at high temperatures, a critical behavior near the Lifshitz point (studied by thermal diffusivity) similar to the one predicted in the case of systems with short range interactions. At low temperatures, a quantum critical behavior in $\text{Pb}_2\text{P}_2\text{S}_6$ crystal can be established by the nonlinear coupling between polar and antipolar fluctuations. An increase in thermal conductivity is induced by Ge impurity in $\text{Pb}_2\text{P}_2\text{S}_6$ crystal, which is explained through the weakening of the acoustic phonons resonance scattering by soft optic phonons because of the appearance of ferroelectric phase polar clusters.

PACS numbers: 64.60.Fr, 64.60.Kw, 65.40.b, 77.22.Ch

I. INTRODUCTION

It was earlier found¹ that Ge doping shifts the second order phase transition ($\text{P}2_1/\text{c} \leftrightarrow \text{Pc}$) in uniaxial ferroelectric $\text{Sn}_2\text{P}_2\text{S}_6$ crystal toward higher temperatures. The increase of the phase transition temperature under the influence of Ge impurities is also known for $\text{Pb}_{1-x}\text{Ge}_x\text{Te}$ and $\text{Sn}_{1-x}\text{Ge}_x\text{Te}$ ferroelectrics,² what demonstrates the universal property of Ge impurities in tin or lead containing hosts of elevating the ferroelectric phase transition temperature. By means of X-ray photoelectron spectroscopy, together with first-principles calculations of electronic spectra, it was found³ that the germanium impurity in $\text{Sn}_2\text{P}_2\text{S}_6$ improves the stereoactivity of the cation sublattice. In $\text{Sn}_2\text{P}_2\text{S}_6$ ferroelectrics the Sn^{2+} cations stereoactivity and the $P^{4+} + P^{4+} \leftrightarrow P^{3+} + P^{5+}$ charge disproportionation is related to the nature of the second order phase transition with mixed displacive-order/disorder character.^{4,5}

While germanium can only be introduced up to a certain quantity,¹ lead can completely substitute tin in $(\text{Pb}_y\text{Sn}_{1-y})_2\text{P}_2\text{S}_6$ and $(\text{Pb}_y\text{Sn}_{1-y})_2\text{P}_2\text{Se}_6$ continuous solid solutions.⁶ The replacement of tin by lead in the cationic sublattice induces the lowering of the phase transition temperature (see Fig. 1), changing its character to a discontinuous transition across the tricritical point (TCP), and stabilizing the paraelectric phase in the ground state (at $T = 0$ K) for $y > 0.61$.⁷ The addition of Pb has the effect of diluting the stereoactivity as it weakens the bonding hybridization responsible for ferroelec-

tricity. Formally, the introduction of lead atoms creates a chemical pressure with similar effects to the mechanical pressure.⁵ The properties of the $(\text{Pb}_y\text{Sn}_{1-y})_2\text{P}_2\text{S}_6$ mixed crystals have been described⁷ within the framework of Blume-Emery-Griffith (BEG) model^{8,9} taking into account the presence of random fields created when substituting tin by lead.

The substitution of S by Se in the anionic sublattice provokes the appearance of an incommensurate (IC) phase at the Lifshitz point (LP) for $x > x_{\text{LP}} \approx 0.28$ in $\text{Sn}_2\text{P}_2(\text{Se}_x\text{S}_{1-x})_6$ solid solutions.¹⁰ The line of tricritical points meet with the line of Lifshitz points at the tricritical Lifshitz point on the $T - x - y$ phase diagram with an interesting topology.¹¹

In mixed crystals $(\text{Pb}_y\text{Sn}_{1-y})_2\text{P}_2\text{S}_6$ and $(\text{Pb}_y\text{Sn}_{1-y})_2\text{P}_2\text{Se}_6$ at $y > 0.61$ and $y > 0.65$, respectively, the paraelectric phase is stable in the ground state,^{6,12} and pure compounds $\text{Pb}_2\text{P}_2\text{S}_6$ and $\text{Pb}_2\text{P}_2\text{Se}_6$ are quantum paraelectrics. The quantum paraelectric state is manifested in the $\text{Pb}_2\text{P}_2\text{S}_6$ crystal by the growth of the dielectric susceptibility while cooling down to 0 K.⁵ A similar state also appears in the $\text{Sn}_2\text{P}_2\text{S}_6$ crystal at hydrostatic pressure $p > 1.5$ GPa.^{13,14}

The Pb^{2+} cations have a smaller stereoactivity compared with Sn^{2+} and this determines the suppression of ferroelectricity while substituting tin by lead.^{5,15} In the case of Ge^{2+} cations, the stereoactivity is bigger, which provokes a temperature rise in the ferroelectric phase transition in $\text{Sn}_2\text{P}_2\text{S}_6$ crystals with germanium impurity.^{1,16} For $\text{Sn}_2\text{P}_2(\text{Se}_x\text{S}_{1-x})_6$ solutions, both S by

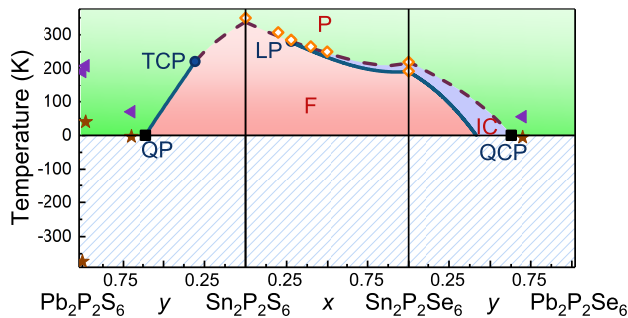


FIG. 1. Phase diagram temperature-composition for mixed crystals in $\text{Sn(Pb)}_2\text{P}_2\text{S(Se)}_6$ system.⁶ Phase transitions in crystals with Ge impurity denote orange rhombs.^{1,16,17} For crystals with quantum paraelectric state determined by Eq. (1) values of T_C (brown stars) and T_1 (violet triangles) are shown. Filled circle denote tricritical point (TCP). Black squares denote quantum point (QP) for the line of first order paraelectric-ferroelectric transitions, and quantum critical point (QCP) for the line of second order paraelectric-incommensurate transitions. Paraelectric (P), ferroelectric (F) and incommensurate (IC) phases are also shown. First order phase transition lines shown by solid lines, second order ones — by dashed lines.

Se and Sn by Ge replacements increase the crystal lattice covalence, and the critical anomaly near the LP becomes sharper.¹⁷

In the case of the binary compounds GeS, SnS, PbS or GeSe, GeTe, it was demonstrated that it is mostly the energy difference between s orbitals of metal atoms and p orbital of chalcogen atoms which determines the stereoactivity of the cations and the crystal lattice covalency.¹⁸ For ternary compounds, for example BiNiO_3 , it was demonstrated¹⁹ that the energy positions of the valence orbitals of the two cations Bi^{4+} and Ni^{2+} are also important. Therefore, for compounds of the $\text{Sn(Pb)}_2\text{P}_2\text{S(Se)}_6$ system with two types of cations (tin or lead metals and phosphorous), a more complex role of the electron valence orbitals hybridization can also be important.^{5,15,20} It was found⁵ that Sn by Pb substitution changes the local potential for spontaneous polarization fluctuation at almost constant intercell interactions. On S by Se substitution, on the contrary, the intersite interaction is changed.

In previous investigations^{5,6,12} the influence of $\text{Sn} \rightarrow \text{Pb}$ and $\text{S} \rightarrow \text{Se}$ substitutions on the phase transition from the paraelectric phase into the ferroelectric one has been analyzed. Here we will pay attention to understanding the germanium impurity influence on the phase transitions and the quantum paraelectric state in different segments of the $\text{Sn(Pb)}_2\text{P}_2\text{S(Se)}_6$ ferroelectrics phase diagram. The temperature dependence of dielectric susceptibility and thermal diffusivity are analyzed with the use of the quantum anharmonic oscillators (QAO) model^{5,21} for the calculation of the spontaneous polarization fluctuations spectra in the local three-well potential. The appear-

ance of the quantum critical behavior in $\text{Pb}_2\text{P}_2\text{S}_6$ and $(\text{Pb}_{0.98}\text{Ge}_{0.02})_2\text{P}_2\text{S}_6$ crystals, in mixed $(\text{Pb}_y\text{Sn}_{1-y})_2\text{P}_2\text{S}_6$ and $(\text{Pb}_y\text{Sn}_{1-y})_2\text{P}_2\text{Se}_6$ crystals with 5% of Ge impurity is investigated, together with the appearance of polar ordering at low temperatures induced by germanium.

II. EXPERIMENTAL DATA

We have investigated the temperature dependence of the dielectric susceptibility with a HP4284 precision LCR meter at temperatures from 300 to 20 K during the cooling cycle at a rate of about 1 K/min, and at frequencies ranging from 20 to 1 MHz.^{22,23} The thermal diffusivity D measurements have been performed by a high resolution ac photopyroelectric calorimetry technique in the standard back detection configuration. A closed cycle He cryostat operated in cooling and heating modes has been used.¹⁶ Ge-doped single crystals were obtained by vapor-transport method in a quartz tube using SnI_2 as a transport agent. The synthesis of the starting material in the polycrystalline form was carried out using high-purity (99.999%) elements.^{16,24} The samples were characterized and oriented by X-ray diffraction technique. For complex dielectric susceptibility measurements, the monocrystal plates with the thickness of about 2 mm and plane parallel faces around 15 mm^2 with silver paste electrodes on polar (100) faces were prepared. For thermal diffusivity measurements all samples have been prepared in the form of thin plane-parallel slabs with thicknesses in a range of 0.500-0.550 mm and whose faces were cut in the monoclinic symmetry plane.

For $\text{Pb}_2\text{P}_2\text{S}_6$ crystal the $\varepsilon'(T)$ dependence shows monotonic rise at cooling till 20 K (see Fig. 2) with some flattening below 50 K. At lead by germanium substitution (about 2%), a clear maximum of $\varepsilon''(T)$ near 35 K (at 100 kHz frequency) is observed (see Fig. 3) and below this temperature $\varepsilon'(T)$ displays frequency dependency in the range between 1 kHz and 1 MHz. In the case of $(\text{Pb}_{0.7}\text{Sn}_{0.25}\text{Ge}_{0.05})_2\text{P}_2\text{S}_6$ and $(\text{Pb}_{0.7}\text{Sn}_{0.25}\text{Ge}_{0.05})_2\text{P}_2\text{Se}_6$ mixed crystals, $\varepsilon'(T)$ and $\varepsilon''(T)$ anomalies also appear in the temperature region of 20–50 K (see Fig. 4, 5). These anomalies are induced by germanium impurity.

By the previous dielectric investigations¹² it was shown that for $(\text{Pb}_y\text{Sn}_{1-y})_2\text{P}_2\text{S}_6$ mixed crystals with $y = 0.61$ and $y = 0.66$ in the paraelectric phase $\varepsilon'(T) \sim (T - T_C)^{-2}$. Such dependence was attributed to glassy-like dielectric susceptibility behavior in $(\text{Pb}_y\text{Sn}_{1-y})_2\text{P}_2\text{S}_6$ mixed crystals with coexisting paraelectric and ferroelectric states. We have shown that such temperature dependence of the dielectric susceptibility can be attributed to the appearance of the spontaneous polarization quantum fluctuations at low temperatures in the crystals of the investigated system.

For $\text{Pb}_2\text{P}_2\text{S}_6$ crystal the real part of the dielectric susceptibility increases monotonously with decreasing temperature and in the measured temperature range the saturation behavior is not observed [see Fig. 2(a)]. In the

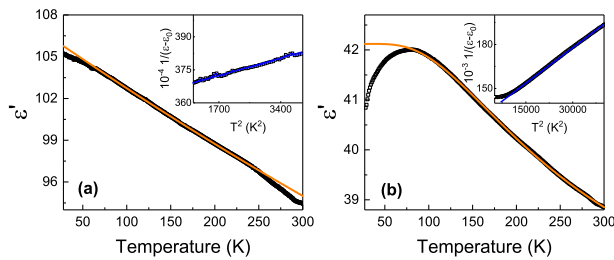


FIG. 2. Temperature dependence of (a) the real part of dielectric susceptibility for $\text{Pb}_2\text{P}_2\text{S}_6$ crystal at 100 kHz and (b) $(\text{Pb}_{0.98}\text{Ge}_{0.02})_2\text{P}_2\text{S}_6$ at 10 kHz. Orange lines are the fitting of Eq. (1). The inset shows the $\epsilon(T)^{-1} \sim T^2$ behavior (blue lines).

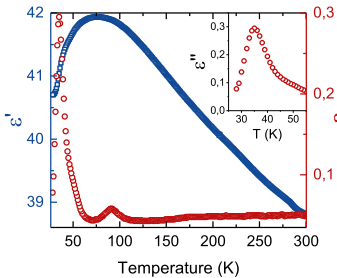


FIG. 3. Temperature dependence of dielectric susceptibility real ϵ' (blue squares) and imaginary ϵ'' (red circles) parts at 100 kHz for $(\text{Pb}_{0.98}\text{Ge}_{0.02})_2\text{P}_2\text{S}_6$ crystal.

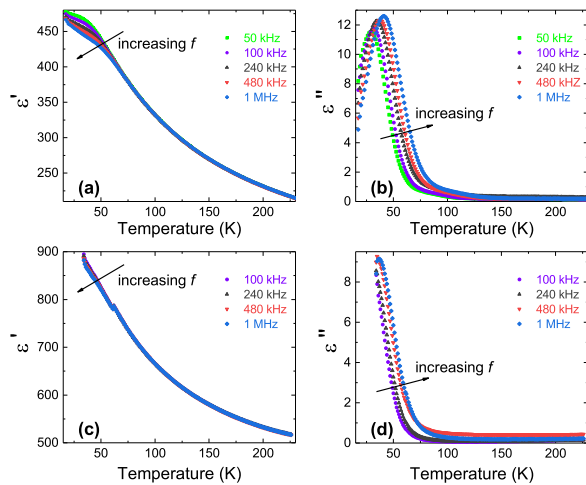


FIG. 4. Temperature dependence of the real and imaginary parts of dielectric susceptibility at different frequencies f of applied field for (a, b) $(\text{Pb}_{0.7}\text{Sn}_{0.25}\text{Ge}_{0.05})_2\text{P}_2\text{S}_6$ and (c, d) $(\text{Pb}_{0.7}\text{Sn}_{0.25}\text{Ge}_{0.05})_2\text{P}_2\text{Se}_6$ crystals.

quantum critical regime the usual Curie-Weiss law of the inverse dielectric susceptibility $1/\epsilon(T) \sim T$ changes into $1/\epsilon(T) \sim T^2$.^{25,26} That is the most prominent criterion for quantum critical behavior. For $\text{Pb}_2\text{P}_2\text{S}_6$ the inverse dielectric susceptibility $1/\epsilon(T)$ exhibits the expected non-classical T^2 temperature dependence over the temperature range 50 K–250 K.

In order to describe the temperature dependencies of the dielectric susceptibility of quantum paraelectrics,

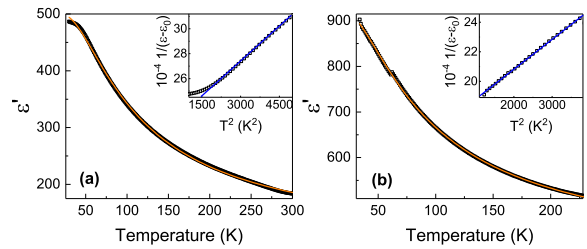


FIG. 5. Temperature dependence of dielectric susceptibility real part of (a) $(\text{Pb}_{0.7}\text{Sn}_{0.25}\text{Ge}_{0.05})_2\text{P}_2\text{S}_6$ and (b) $(\text{Pb}_{0.7}\text{Sn}_{0.25}\text{Ge}_{0.05})_2\text{P}_2\text{Se}_6$ at 10 kHz; orange solid curve is the fitting according to the Barret's equation (1). The inset shows the reciprocal dielectric susceptibility as a function of the squared temperature (blue lines).

Barretts equation can be used:

$$\epsilon(T) = \frac{C}{\left(\frac{T_1}{2}\right) \coth\left(\frac{T_1}{2T}\right) - T_C} + \epsilon_0, \quad (1)$$

where C is the Curie-Weiss constant, T_C is the classical paraelectric Curie temperature, ϵ_0 is a temperature independent constant and T_1 is the dividing point between the low temperatures where quantum effects are important so $\epsilon(T)$ deviates from Curie-Weiss law, and the high temperature region where a classical approximation and Curie-Weiss law are valid.^{25,27}

In many cases, $T_C \leq 0$ K, and the material does not undergo a ferroelectric phase transition at any finite temperature. When T_C is finite and $T_C < T_1$, the quantum fluctuations break the long range ferroelectric order and stabilize the quantum paraelectric state in the sample. Probable ferroelectric transition occurs at T_C .²⁸ According to dielectric data of $\text{Pb}_2\text{P}_2\text{S}_6$ [see Fig. 2(a)] deviation from Barret's equation starts around 75 K. The obtained parameter values ($T_1 \approx 190$ K and $T_C \approx -370$ K) for $\text{Pb}_2\text{P}_2\text{S}_6$ crystal demonstrate that the material does not undergo a ferroelectric phase transition at any finite temperature.

As was mentioned above, when Pb substitutes Sn in $\text{Sn}_2\text{P}_2\text{S}_6$ type crystals, the hybridization of anion and cation sublattices electron orbitals becomes weaker, reducing the phase transition temperature. On the other hand, Ge dopant plays an opposite role: it enhances the total stereoactivity of the cation sublattice in the crystal. Small amount of impurities in quantum paraelectrics could induce ferroelectricity.^{29,30} So, it is possible that germanium impurities can affect quantum paraelectric state of $\text{Pb}_2\text{P}_2\text{S}_6$. Figure 2(b) shows the temperature dependence of the real part of dielectric susceptibility for $(\text{Pb}_{0.98}\text{Ge}_{0.02})_2\text{P}_2\text{S}_6$ crystal and confirms a non-classical T^2 behavior of the inverse dielectric susceptibility. For this, the temperature dependence of the real part of dielectric susceptibility for crystal doped by germanium is fitted by the Barretts equation (1) giving temperatures $T_1 \approx 200$ K and $T_C \approx 40$ K. Since $T_C < T_1$ for $(\text{Pb}_{0.98}\text{Ge}_{0.02})_2\text{P}_2\text{S}_6$, it could be concluded that the

long-range ferroelectric order in the sample doped by Ge is broken due to quantum fluctuations below 200 K, and a probable ferroelectric transition occurs in the temperature region between 40 K and 80 K (see Fig. 3). Doping with germanium decreases the real part of susceptibility below 80 K deviating from Barrett's fit [see Fig. 2(b)].

The peak of the real part of the dielectric susceptibility is broad. Moreover, there are two peaks of the imaginary part of the dielectric susceptibility with a frequency dispersive behavior, and the temperatures of the loss peaks are around 50 K and 100 K at 100 kHz (see Fig. 3). Obviously, this is related to compositional fluctuations in $(\text{Pb}_{0.98}\text{Ge}_{0.02})_2\text{P}_2\text{S}_6$ crystal. Also, a fast-enough dynamics of local dipoles, and slower dynamics of noninteracting ones, or weakly interacting nanoclusters, can determine the broadness of the phase transition induced by Ge impurity with related frequency–temperature anomalous behavior of dielectric susceptibility that is similar to the one observed in the case of a crossover between dipole glass and ferroelectric relaxor.^{29,30}

As was already mentioned, for $(\text{Pb}_y\text{Sn}_{1-y})_2\text{P}_2\text{S}_6$ mixed crystals with compositions $y = 0.61$ and $y = 0.66$, which are close to the transition at zero temperature from a polar phase to a paraelectric one, the dielectric susceptibility demonstrates the quantum critical behavior with $T_C \approx 35$ K and 20 K, respectively.¹² We have investigated the influence of Ge dopants on the quantum paraelectric state of $\text{Pb}_2\text{P}_2\text{S}_6$ type compounds by studying of $(\text{Pb}_{0.7}\text{Sn}_{0.25}\text{Ge}_{0.05})_2\text{P}_2\text{S}_6$ and $(\text{Pb}_{0.7}\text{Sn}_{0.25}\text{Ge}_{0.05})_2\text{P}_2\text{Se}_6$ samples. In these crystals the Sn^{2+} sites of pure $\text{Sn}_2\text{P}_2\text{S}_6$ were codoped with two different impurities (Pb^{2+} and Ge^{2+}) which have very different influences on the phase transitions. It is important to realize that Sn substitution has the strongest effect because the ferroelectric phase transition is induced by the stereoactivity of the Sn^{2+} cation $5s^2$ electron lone pair.

The temperature dependence of the real part of the dielectric susceptibility for $(\text{Pb}_{0.7}\text{Sn}_{0.25}\text{Ge}_{0.05})_2\text{P}_2\text{S}_6$ and $(\text{Pb}_{0.7}\text{Sn}_{0.25}\text{Ge}_{0.05})_2\text{P}_2\text{Se}_6$ crystals is shown in Fig. 4. Susceptibility ϵ' increases continuously with decreasing temperature from room temperature till 20 K. The dielectric losses have maximum at low temperature, around 40 K at frequency 1 MHz. The inverse dielectric permittivity $1/\epsilon(T)$ exhibits the expected non-classical T^2 temperature dependence not only in the case of doped $(\text{Pb}_{0.98}\text{Ge}_{0.02})_2\text{P}_2\text{S}_6$ sample (see Fig. 2), but it is also observed in mixed crystals $(\text{Pb}_{0.7}\text{Sn}_{0.25}\text{Ge}_{0.05})_2\text{P}_2\text{S}_6$ and $(\text{Pb}_{0.7}\text{Sn}_{0.25}\text{Ge}_{0.05})_2\text{P}_2\text{Se}_6$ (see Fig. 5). From this follows that the ferroelectric quantum critical behavior is relatively insensitive to quenched disorder in doped samples and mixed crystals.

By fitting the experimental data of Fig. 5(a) to Barrett's equation (1) it was determined the next parameters: $T_1 \approx 70$ K, $T_C \approx -4$ K, and $C \approx 30670$ K. The observed temperature behavior of the dielectric susceptibility demonstrates that $(\text{Pb}_{0.7}\text{Sn}_{0.25}\text{Ge}_{0.05})_2\text{P}_2\text{S}_6$ crystal obviously undergoes some inhomogeneous polar ordering at very low temperatures.

Similarly, the temperature dependence of the dielectric susceptibility $\epsilon'(T)$ for the $(\text{Pb}_{0.7}\text{Sn}_{0.25}\text{Ge}_{0.05})_2\text{P}_2\text{Se}_6$ crystal is shown in Fig. 5(b). On cooling from 300 till 20 K both ϵ' and ϵ'' increase, their frequency dispersion more clearly appears below 100 K.²³ By fitting to the Barrett's equation (1) [see Fig. 5(b)] it was found that $T_1 \approx 55$ K, $T_C \approx -6$ K, and $C \approx 34260$ K. It is seen that in the selenide mixed crystal $(\text{Pb}_{0.7}\text{Sn}_{0.25}\text{Ge}_{0.05})_2\text{P}_2\text{Se}_6$ the germanium impurity induces inhomogeneous polar ordering at lower temperatures similarly to the case of the sulfide analogue.

As a whole, according to the results of the dielectric investigations, it can be concluded that $\text{Pb}_2\text{P}_2\text{S}_6$ crystals exhibit a quantum paraelectric state. The introduction of small amounts of germanium dopant provokes the appearance of the ferroelectric phase. In mixed crystals a very inhomogeneous polar ordering (like dipole glassy or relaxor state) appears below approximately 100 K.

We can see that the $\epsilon'(T)$ dependence of Eq. (1), considering quantum fluctuations for $\text{Pb}_2\text{P}_2\text{S}_6$ compound, predicts the value of T_C in accordance with $T_0(y)$ dependence for $(\text{Pb}_y\text{Sn}_{1-y})_2\text{P}_2\text{S}_6$ mixed crystals (see Fig. 1). At this, the value of T_1 is strongly suppressed in mixed crystals — from 190 K in $\text{Pb}_2\text{P}_2\text{S}_6$ and 207 K in the case of $(\text{Pb}_{0.98}\text{Ge}_{0.02})_2\text{P}_2\text{S}_6$ to $T_1 \approx 70$ K in the solution with $y = 0.7$. Such decrease of the crossover temperature T_1 from classic to quantum fluctuations behavior can be interpreted as the manifestation of quantum coherence destruction for the electronic component of spontaneous polarization fluctuations, that are determined by phosphorous cations $P^{4+} + P^{4+} \leftrightarrow P^{3+} + P^{5+}$ charge disproportionation. The electronic contribution to spontaneous polarization is connected to the coherent state of polaronic excitons — small hole polarons in SnPS_3 structural groups are coupled with small electronic polarons in nearest SnPS_3 structural groups.^{5,31} Obviously such polaronic excitons are strongly bounded by defects in mixed crystals what preserves the development of quantum fluctuations when lowering the temperature.

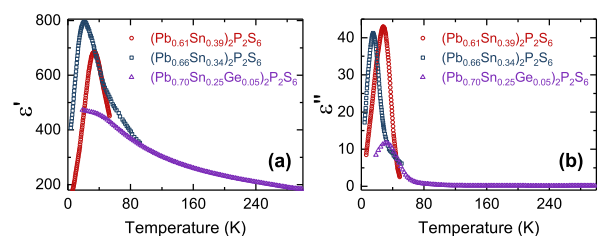


FIG. 6. Temperature dependence of dielectric susceptibility (a) real and (b) imaginary parts for crystals $(\text{Pb}_{0.7}\text{Sn}_{0.25}\text{Ge}_{0.05})_2\text{P}_2\text{S}_6$. Data [12] for $(\text{Pb}_{0.61}\text{Sn}_{0.39})_2\text{P}_2\text{S}_6$ and $(\text{Pb}_{0.66}\text{Sn}_{0.34})_2\text{P}_2\text{S}_6$ mixed crystals are also shown for comparison.

In Fig. 6 the temperature dependencies of real and imaginary parts of dielectric susceptibility are compared for $(\text{Pb}_{0.7}\text{Sn}_{0.25}\text{Ge}_{0.05})_2\text{P}_2\text{S}_6$ crystal in comparison with data [12] for $(\text{Pb}_{0.66}\text{Sn}_{0.34})_2\text{P}_2\text{S}_6$ and

(Pb_{0.61}Sn_{0.39})₂P₂S₆ mixed crystals. We can see that the dielectric anomalies induced by the germanium impurity are smeared similarly to the observed anomalies in the case of (Pb_{*y*}Sn_{1-*y*})₂P₂S₆ solid solutions with lead concentration near the threshold value of *y*. In all three samples a complex thermal evolution of the provoked inhomogeneous polarization occurs on cooling below 100 K.

The thermal properties of Sn₂P₂S₆ and (Sn_{0.95}Ge_{0.05})₂P₂S₆, Sn₂P₂(Se_{0.28}S_{0.72})₆ and (Sn_{0.95}Ge_{0.05})₂P₂(Se_{0.28}S_{0.72})₆, Pb₂P₂S₆ and (Pb_{0.98}Ge_{0.02})₂P₂S₆, (Pb_{0.7}Sn_{0.25}Ge_{0.05})₂P₂S₆ and (Pb_{0.7}Sn_{0.25}Ge_{0.05})₂P₂Se₆ single crystals have been studied by means of *ac* photopyroelectric calorimetry, measuring the thermal diffusivity.^{16,17,32–34} Thermal conductivity *k* has been retrieved by combining the experimental thermal diffusivity *D* and the calculated background heat capacity *c* for Sn₂P₂S₆, Pb₂P₂S₆ and the experimental one for Sn₂P₂Se₆, Pb₂P₂Se₆.^{35,36} The detailed procedure to obtain the thermal conductivity is explained elsewhere.³⁷

For Sn₂P₂S₆ crystal, the germanium dopant shifts the temperature of continuous ferroelectric transition upwards and sharpens the critical anomaly of thermal diffusivity (see Fig. 7).¹⁶ The introduction of germanium impurity into Sn₂P₂S₆ crystal lattice increases the dip of the thermal diffusivity anomaly near the second order phase transition, which becomes a little broader than in the case of the nominally pure crystal [see Fig. 7(b)] and therefore, it was not possible to perform fittings with great accuracy.^{16,33}

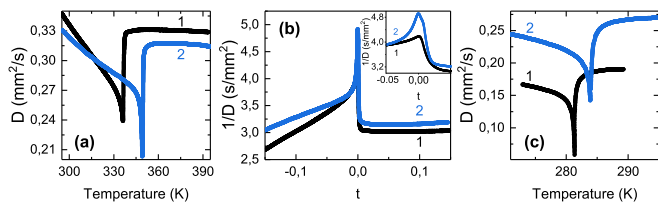


FIG. 7. Temperature dependence of Sn₂P₂S₆ (1) and (Sn_{0.95}Ge_{0.05})₂P₂S₆ (2) crystals (a) thermal diffusivity *D* and (b) their reciprocal value as a function of reduced temperature $t = (T - T_c)/T_c$; (c) thermal diffusivity *D* temperature anomalies near the Lifshitz point in Sn₂P₂(Se_{0.28}S_{0.72})₆ (1) and (Sn_{0.95}Ge_{0.05})₂P₂(Se_{0.28}S_{0.72})₆ (2) crystals.^{16,32–34}

For the Lifshitz point composition Sn₂P₂(Se_{0.28}S_{0.72})₆, the critical index $\alpha \approx 0.34$ and the critical amplitudes ratio $A^+/A^- \approx 0.42$ were observed.³⁴ The introduction of Ge increases the critical temperature from 281.3 K to 284 K [see Fig. 7(c)] but changes neither the character of the transition nor the universality class, as it is uniaxial Lifshitz class with critical exponent $\alpha \approx 0.25$ and $A^+/A^- \approx 0.49$.³² Such values agree with the theoretical ones estimated for a Lifshitz system without considering strong dipolar interactions. In the case of the Lifshitz point in uniaxial ferroelectrics only small multiplicative corrections to mean field behavior are expected³⁸ in the critical region. Hence, both the critical expo-

nent and the amplitude ratio values observed for the Sn₂P₂(Se_{0.28}S_{0.72})₆ mixed crystal lead to the conclusion that long-range interactions do not have a strong influence on the critical behavior in this system. This can be related to the partial screening of the dipole-dipole interaction by charge carriers in the Sn₂P₂(Se_{*x*}S_{1-*x*})₆ ferroelectric semiconductors.

In order to determine the thermal conductivity *k* of the investigated samples, thermal diffusivity data *D* have been combined with heat capacity data *c* using the following equation

$$k = cD. \quad (2)$$

For (Pb_{0.98}Ge_{0.02})₂P₂S₆ crystal the thermal conductivity at low temperatures is bigger than in the case of pure Pb₂P₂S₆ crystal (see Fig. 8). This is related to the induction of polar clusters of the ferroelectric phase when doping with Ge. The dielectric susceptibility of such clusters is smaller than the susceptibility of the paraelectric phase and the frequency of the lowest energy soft polar optic mode near the Brillouin zone (BZ) center is elevated. The growth of the soft optical mode frequency diminishes the probability of the optical phonon resonance scattering by acoustic phonons.^{39,40} At low temperatures heat is transferred by acoustic and lowest frequency optical phonons. Acoustic phonons with small wave numbers are involved mostly in normal scattering (N-process) that doesn't contribute to thermal resistivity. The phonons from the optical branch near the BZ center also participate in Umklapp scattering (U-process) by lattice imperfections, which provide an effective thermal resistivity. So, the hardening of the optical branch lowers the population of the optical phonons and increases the thermal conductivity of (Pb_{0.98}Ge_{0.02})₂P₂S₆ crystal at very low temperatures (see Fig. 8).

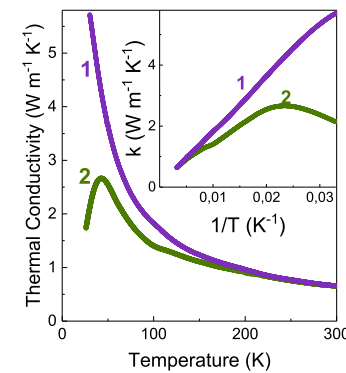


FIG. 8. Temperature dependence of thermal conductivity *k* for (Pb_{0.98}Ge_{0.02})₂P₂S₆ (1) and Pb₂P₂S₆ (2) crystals. Inset: their $k(T^{-1})$ dependence. Data for *D* is taken from [41].

Such explanation agrees with the comparison of the changes in the temperature dependencies of dielectric susceptibility and thermal conductivity induced by germanium (Fig. 9). On cooling below 100 K, the difference in thermal conductivity between (Pb_{0.98}Ge_{0.02})₂P₂S₆ and Pb₂P₂S₆ crystals rapidly rises, and oppositely — dielectric susceptibility of (Pb_{0.98}Ge_{0.02})₂P₂S₆ crystal quickly lowers relatively to Pb₂P₂S₆ crystal susceptibility.

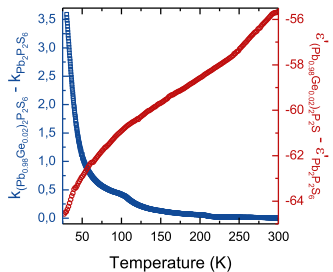


FIG. 9. Temperature dependence of thermal conductivity k and dielectric susceptibility ϵ' difference for $(\text{Pb}_{0.98}\text{Ge}_{0.02})_2\text{P}_2\text{S}_6$ and $\text{Pb}_2\text{P}_2\text{S}_6$ crystals. Data for D is taken from [41].

Such low temperature evolution of the dielectric susceptibility induced by germanium impurity reflects the hardening (frequency increase) of the lowest polar optic mode near the BZ center.

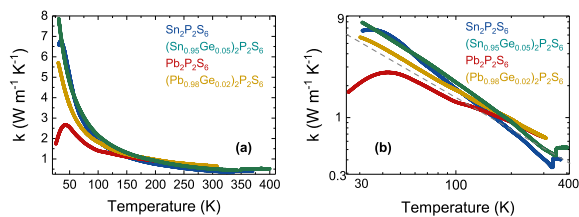


FIG. 10. Temperature dependence of thermal conductivity k for $\text{Sn}_2\text{P}_2\text{S}_6$, $(\text{Sn}_{0.95}\text{Ge}_{0.05})_2\text{P}_2\text{S}_6$, $\text{Pb}_2\text{P}_2\text{S}_6$ and $(\text{Pb}_{0.98}\text{Ge}_{0.02})_2\text{P}_2\text{S}_6$ in (a) normal coordinates and (b) in log-log scale. Grey dashed curve shows $k \sim T^{-1}$ behavior. Data for D is taken from [17, 33, 34, and 41].

With the introduction of germanium into the lattice of $\text{Pb}_2\text{P}_2\text{S}_6$ crystal, the temperature dependence of the thermal conductivity coefficient $k(T)$ in a wide temperature range coincides with Eikens law, i.e. it is proportional to the inverse of temperature (see Fig. 10). Such dependency gives evidence about the dominant role of three-phonon scattering processes in the thermal resistivity. In the case of $\text{Sn}_2\text{P}_2\text{S}_6$ ferroelectric phase, the introduction of Ge impurity also improves $k \sim T^{-1}$ temperature dependence for the thermal conductivity.

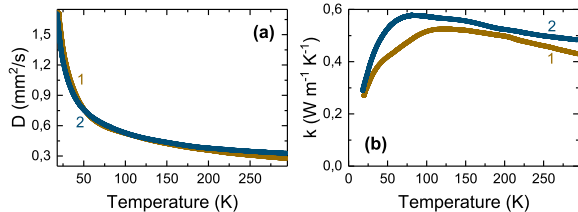


FIG. 11. Temperature dependence of (a) thermal diffusivity D and (b) thermal conductivity k for $(\text{Pb}_{0.7}\text{Sn}_{0.25}\text{Ge}_{0.05})_2\text{P}_2\text{S}_6$ (1) and $(\text{Pb}_{0.7}\text{Sn}_{0.25}\text{Ge}_{0.05})_2\text{P}_2\text{Se}_6$ (2) mixed crystals.

In the case of $(\text{Pb}_{0.7}\text{Sn}_{0.25}\text{Ge}_{0.05})_2\text{P}_2\text{S}_6$ mixed crystals the thermal conductivity temperature behavior (see Fig. 11) is similar to observed in case of glassy materials, what demonstrates an effective phonon scattering

in solid solutions with sublattice of mixed tin and lead cations. The addition of germanium impurity induces the dipole glass state, which appeared in the complex dielectric susceptibility frequency dependency below 100 K (see Fig. 4). Only a small contribution to thermal conductivity by germanium addition is observed in the temperature range from 50 K to 120 K. Similar behavior is also observed for $(\text{Pb}_{0.7}\text{Sn}_{0.25}\text{Ge}_{0.05})_2\text{P}_2\text{Se}_6$ selenide solid solution.

III. DISCUSSION OF RESULTS

With the application of the local mode approach to the monoclinic ferroelectrics $\text{Sn}_2\text{P}_2\text{S}_6$, it was found⁴ a three-well potential energy surface. The nonlinear interaction of the vibration modes leads to this complex shape of local potential for spontaneous polarization fluctuations. Such nonlinearity is a result of significant electron-phonon interaction, that can be described as a second order Jahn-Teller effect related to the electron lone pair stereoactivity of Sn^{2+} cations.^{4,15} The nonlinear lattice dynamics is reflected in the theoretically and experimentally observed^{6,21} complex nature of the soft mode related to continuous phase transition.

In the description of the microscopic origin of $\text{Sn}_2\text{P}_2\text{S}_6$ ferroelectric lattice instability, in addition to the second order Jahn-Teller effect, the $P^{4+} + P^{4+} \leftrightarrow P^{3+} + P^{5+}$ charge disproportionation was also considered.⁵ Such electronic correlations can be described within the presentation of Andersons electron pairs flipping, and thermodynamics of $\text{Sn}_2\text{P}_2\text{S}_6$ family ferroelectrics can be considered within the framework of BEG model.^{20,42,43} In this approximation, a change in the local three-well potential by flattening the side wells leads to a decrease of the calculated continuous phase transition temperature and a TCP is reached. Below TCP temperature, the first order ferroelectric phase transition line further drops down to 0 K. In the case of the family of $\text{Sn}_2\text{P}_2\text{S}_6$ ferroelectric crystals, such an evolution can be induced substituting tin by lead in mixed crystals $(\text{Pb}_y\text{Sn}_{1-y})_2\text{P}_2\text{S}_6$ or under hydrostatic compression.⁵

The QAO model with the description of electronic recharging and lattice instability as pseudospin fluctuations in an anharmonic potential of three-well shape was proposed for a description of the temperature-pressure diagram of $\text{Sn}_2\text{P}_2\text{S}_6$ and of the temperature-composition diagram of $(\text{Pb}_y\text{Sn}_{1-y})_2\text{P}_2\text{S}_6$ ferroelectric mixed crystals.⁵ In the QAO model, the real crystal lattice is represented as a system of one-dimensional interacting quantum anharmonic oscillators. A shape of the phase diagram calculated for the BEG model [see Fig. 12(a)] correlates with the experimental observations. Here the on-site energy Δ changes with the variation of crystals chemical composition at almost constant intersite interaction J . The dimensionless parameter $\delta = \Delta/J$ was estimated by using the following characteristics of the $(\text{Pb}_y\text{Sn}_{1-y})_2\text{P}_2\text{S}_6$ mixed crystals $T - \delta$ phase dia-

gram: the second order phase transition temperature for $\text{Sn}_2\text{P}_2\text{S}_6$ crystal, the coordinates of tricritical points on temperature-composition $T-y$ diagram, the composition y at which the phase transition temperature goes down to zero.^{5,7} The shape of the local potential was determined with known values of on-site energy Δ [see Fig. 12(b)].

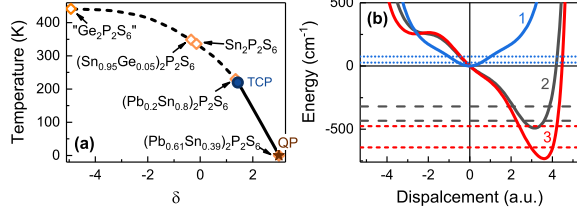


FIG. 12. (a) the phase transition temperature as a function of $\delta = \Delta/J$, calculated in the mean-field approximation on the BEG model⁵ with shown points for $\text{Ge}_2\text{P}_2\text{S}_6$, $(\text{Sn}_{0.95}\text{Ge}_{0.05})_2\text{P}_2\text{S}_6$, $\text{Sn}_2\text{P}_2\text{S}_6$, $(\text{Pb}_{0.2}\text{Sn}_{0.8})_2\text{P}_2\text{S}_6$ and $(\text{Pb}_{0.61}\text{Sn}_{0.39})_2\text{P}_2\text{S}_6$ crystals. Solid line denotes first order and dashed one second order phase transitions. Filled circle — TCP, star — QP. (b) the QAO local potentials at $T = 0$ K and their lowest energy levels for crystals $\text{Pb}_2\text{P}_2\text{S}_6$ (1), $\text{Sn}_2\text{P}_2\text{S}_6$ (2) and for virtual crystal $\text{Ge}_2\text{P}_2\text{S}_6$ (3).

The local potentials of quantum anharmonic oscillators for $\text{Pb}_2\text{P}_2\text{S}_6$, $\text{Sn}_2\text{P}_2\text{S}_6$ and virtual $\text{Ge}_2\text{P}_2\text{S}_6$ crystals, which were determined by earlier⁵ described methodology, are shown at Fig. 12(b). They are characterized by below listed values of zero-point energy $E_0 = \hbar\omega_0/2$, related frequency ω_0 and temperature T_x :

$$\begin{aligned} \text{Pb}_2\text{P}_2\text{S}_6 - \omega_0 &\approx 47 \text{ cm}^{-1}, T_x \approx 72 \text{ K}, E_0 \approx 0.003 \text{ eV}; \\ \text{Sn}_2\text{P}_2\text{S}_6 - \omega_0 &\approx 60 \text{ cm}^{-1}, T_x \approx 86 \text{ K}, E_0 \approx 0.004 \text{ eV}; \\ \text{Ge}_2\text{P}_2\text{S}_6 - \omega_0 &\approx 80 \text{ cm}^{-1}, T_x \approx 115 \text{ K}, E_0 \approx 0.005 \text{ eV}; \end{aligned}$$

The shape of the local potential favors an off-center displacement of Sn^{2+} cations in $\text{Sn}_2\text{P}_2\text{S}_6$ or Pb^{2+} cations in $\text{Pb}_2\text{P}_2\text{S}_6$ crystal lattice that induces a local electric dipole. The local dipoles at a given inter-cell interaction J cannot be ordered down to the lowest temperatures in case of $\text{Pb}_2\text{P}_2\text{S}_6$ crystal, but here the ferroelectric ground states may be reached via chemical substitution of lead cations by tin or germanium cations.

At low temperatures for ferroelectrics the quantum fluctuating electrical dipoles are coupled to the elastic steps of freedom. The quantum critical phase in three dimensional space d is evident by the fact that the dielectric susceptibility depends on both the static and dynamic (frequency dependent) properties of the system, which results for multiaxial ferroelectrics, like perovskite SrTiO_3 , in a unity rise of effective dimension — $d_{eff} = d + 1 = 4$.^{27,44} In the uniaxial ferroelectrics apart from short range interactions, the long range anisotropic electrical dipole interactions provide a further unity increase in the effective dimension to $d_{eff} = d + 2 = 5$.^{45,46}

For SrTiO_3 below 25 K a nonmonotonic temperature dependence of dielectric susceptibility arises from optic and acoustic phonon coupling (electrostriction).²⁶ The upturn in the inverse susceptibility occur when T is less than 10% of T_x , where T_x is the temperature associated

with the soft transverse optical phonon frequency ω at the BZ center in the zero-temperature limit. This means that fit of the dielectric susceptibility data to a quantum criticality model without taking into account of electrostrictive coupling is appropriate only for $T > 0.1T_x$. This condition is fulfilled for $\text{Pb}_2\text{P}_2\text{S}_6$ crystal where $0.1T_x \approx 7$ K.

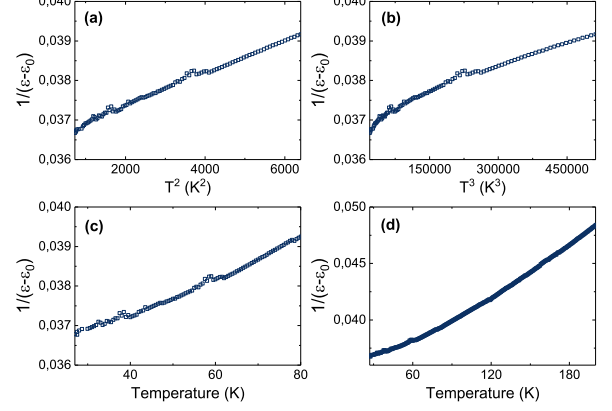


FIG. 13. Reciprocal dielectric susceptibility of $\text{Pb}_2\text{P}_2\text{S}_6$ crystal as a function of temperature in different scales.

We present the measured dielectric susceptibility $1/\epsilon'(T)$ over the range 27–80 K for $\text{Pb}_2\text{P}_2\text{S}_6$ crystal in different temperature scales (see Fig. 13). From the comparison of Fig. 13(a) and Fig. 13(b), it is seen that $1/\epsilon'$ varies as T^2 in the region 27–80 K and doesn't satisfy the T^3 quantum critical behavior. Above 80 K this crystal exhibits classical Curie-Weiss behavior [see Fig. 13(c, d)]. We emphasize that for $\text{Pb}_2\text{P}_2\text{S}_6$ crystal the critical exponent is close to $\gamma = 2.0$, that is calculated and observed for multiaxial quantum critical systems like SrTiO_3 ,^{27,44} and does not follow the theoretically predicted for uniaxial ferroelectrics value $\gamma = 3.0$ ^{45,46} which have been experimentally found in the case of $\text{BaFe}_{12}\text{O}_{19}$ and $\text{SrFe}_{12}\text{O}_{19}$ crystals.⁴⁵

The $1/T^2$ low temperature variation found for the dielectric susceptibility of $\text{Pb}_2\text{P}_2\text{S}_6$ close to the quantum critical point instead of the expected uniaxial behavior of $1/T^3$ can be explained at first glance by a screening phenomenon in semiconductor materials of the $\text{Sn}(\text{Pb})_2\text{P}_2\text{S}(\text{Se})_6$ system which weakens the electric dipole interaction. Such explanation is seen as appropriate for the above discussed critical behavior near the Lifshitz point in $\text{Sn}_2\text{P}_2(\text{Se}_{0.28}\text{S}_{0.72})_6$ mixed crystal, which agrees with the theoretically predicted for systems with short-range interactions.^{17,34} But, for $\text{Pb}_2\text{P}_2\text{S}_6$ crystals at low temperatures, the electric conductivity is very small (below $10\text{--}14 \text{ Om}^{-1} \text{ cm}^{-1}$)⁴⁷ and screening effects cant be effective with a low concentration of the free charge carriers.

Figure 14 demonstrates, that for both $\text{Sn}_2\text{P}_2\text{S}_6$ and $\text{Pb}_2\text{P}_2\text{S}_6$ crystals the soft optic branch in the paraelectric phase is flat: soft phonons frequency slightly changes with the increase of wave number and moves from the

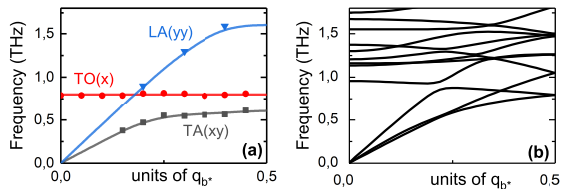


FIG. 14. Acoustic and soft optic phonon branches: (a) determined by neutron scattering at 440 K in paraelectric $P2_1/c$ phase of $\text{Sn}_2\text{P}_2\text{S}_6$; ⁴⁸ (b) calculated GGA approach of DFT for $\text{Pb}_2\text{P}_2\text{S}_6$. ⁵

BZ center to the edge, where the crossing with acoustic phonon branches occurs.⁴⁸ On cooling to the continuous phase transition temperature $T_0 \approx 337$ K for $\text{Sn}_2\text{P}_2\text{S}_6$ crystal, in addition to the development of polar fluctuations near the BZ center, the antipolar fluctuations also strongly develop in the paraelectric phase. Here, critical behavior can be described as a crossover between Ising and XY universality classes, what is expected near bicritical points with coupled polar and antipolar order parameters and competing instabilities in the reciprocal wave vectors space.¹¹ A similar situation obviously exists in the quantum paraelectric phase of $\text{Pb}_2\text{P}_2\text{S}_6$ crystal, where on cooling down to 0 K the flat optic phonon branch softens across wide reciprocal space in BZ. Besides, the long wavelength polar fluctuations grow together with a development of short wavelength antipolar fluctuations and, therefore, their nonlinear coupling can modify the quantum critical behavior.

IV. CONCLUSIONS

The dipole ordering temperature of $\text{Sn}(\text{Pb})_2\text{P}_2\text{S}(\text{Se})_6$ materials may be tuned by chemical substitution realizing a ferroelectric quantum phase transition and quantum glassy or relaxor type phenomena in different parts of the phase diagram. The introduction of Ge impurity initiates several important phenomena: it increases the temperature of the phase transitions and improves the spontaneous polarization in the crystal; it doesn't shift the coordinate of the Lifshitz point x_{LP} in $\text{Sn}_2\text{P}_2(\text{Se}_x\text{S}_{1-x})_6$ mixed crystals; it initiates a more pronounced critical anomaly in $\text{Sn}_2\text{P}_2\text{S}_6$ crystals; it induces the appearance of a phase transition in the quantum paraelectric $\text{Pb}_2\text{P}_2\text{S}_6$ and inhomogeneous polar ordering in $(\text{Pb}_{0.7}\text{Sn}_{0.3})_2\text{P}_2\text{S}(\text{Se})_6$ crystals. The quantum fluctuations are destroyed in the mixed crystals, what follows from the comparison of the low temperature behavior of the thermal diffusivity and the complex dielectric susceptibility at different frequencies.

By means of dielectric measurements it was shown that for $\text{Pb}_2\text{P}_2\text{S}_6$ crystal the real part of the dielectric susceptibility increases monotonously with decreasing temperature in the range from 300 K till 20 K. It was found that in the quantum critical regime the usual Curie-Weiss

law of the inverse of dielectric susceptibility $1/\varepsilon'(T) \sim T$ changes into $1/\varepsilon'(T) \sim T^2$, which is the prominent criterion for quantum critical behavior. The nature of long-range dipole interactions in uniaxial materials predicts a dielectric susceptibility varying as $1/T^3$ close to the quantum critical point. But we found that the dielectric susceptibility varies as $1/T^2$ as expected and observed in better known multi-axial systems. This result can be partially explained by a screening phenomenon in semiconductor materials of the $\text{Sn}(\text{Pb})_2\text{P}_2\text{S}(\text{Se})_6$ system which is effective at relatively high temperatures and weakens the electric dipole interactions. But due to the free charge carriers low concentration at low temperatures, evidently the nonlinear coupling between polar and antipolar fluctuation is surely related to the modification of the observed quantum critical behavior in $\text{Pb}_2\text{P}_2\text{S}_6$ crystal.

The temperature dependence of the dielectric susceptibility has been analyzed in terms of the Barrett model that also demonstrates the presence of a quantum paraelectric state in $\text{Pb}_2\text{P}_2\text{S}_6$ type crystals. Small amounts of germanium impurity in $(\text{Pb}_{0.98}\text{Ge}_{0.02})_2\text{P}_2\text{S}_6$ crystal induce the appearance of the ferroelectric phase, what is manifested in the decrease of the real part of the dielectric susceptibility below 75 K, deviating from the Barrett's fit, and the appearance of a broad peak around 40 K. The observed behavior of the dielectric susceptibility temperature dependence demonstrates that $(\text{Pb}_{0.7}\text{Sn}_{0.3})_2\text{P}_2\text{S}_6 + 5\%$ Ge crystal doesn't undergo a ferroelectric phase transition with polar ordering at macroscopic scale at any finite temperature, implying that a relaxor or dipole glass state appears below 50 K. The temperature dependence of the dielectric susceptibility at different frequencies for $(\text{Pb}_{0.7}\text{Sn}_{0.3})_2\text{P}_2\text{S}_6 + 5\%$ Ge sample is similar to the observed one for the sulfide mixed crystal.

The thermal properties of $\text{Pb}_2\text{P}_2\text{S}_6$, $(\text{Pb}_{0.98}\text{Ge}_{0.02})_2\text{P}_2\text{S}_6$, $(\text{Pb}_{0.7}\text{Sn}_{0.25}\text{Ge}_{0.05})_2\text{P}_2\text{S}_6$ and $(\text{Pb}_{0.7}\text{Sn}_{0.25}\text{Ge}_{0.05})_2\text{P}_2\text{S}_6$ single crystals have been studied, as it was earlier performed for $\text{Sn}_2\text{P}_2\text{S}_6$ crystal doped by germanium,¹⁶ where Ge impurity sharpens the Ising type critical anomaly at the continuous ferroelectric transition. It was found that for $(\text{Pb}_{0.98}\text{Ge}_{0.02})_2\text{P}_2\text{S}_6$ crystal the thermal conductivity at low temperature (near 50 K) is bigger than in the case of pure $\text{Pb}_2\text{P}_2\text{S}_6$ crystal. This is obviously related to the Ge induction of polar clusters of the ferroelectric phase. The dielectric susceptibility of such clusters is smaller than the susceptibility of the paraelectric phase and the frequency of the lowest energy soft optical mode near the BZ center is obviously elevated. The increase in the soft optical mode frequency diminishes the probability of acoustic phonons resonance scattering by optic phonons. At low temperatures, heat is transferred by the acoustic and the lowest frequency optical phonons. Acoustic phonons with the small wave numbers are involved mostly in normal scattering processes that don't contribute to the thermal resistivity. The phonons from the optical branch near the BZ center also participate in Umklapp scattering by lattice imperfections which

provides an effective thermal resistivity. Thus, the hardening of the optical branch lowers the population of the optical phonons and increases the thermal conductivity of $(\text{Pb}_{0.98}\text{Ge}_{0.02})_2\text{P}_2\text{S}_6$ crystal. In the case of $(\text{Pb}_{0.7}\text{Sn}_{0.25}\text{Ge}_{0.05})_2\text{P}_2\text{S}(\text{Se})_6$ mixed crystals, the thermal conductivity behaves on cooling, like in glassy

materials, which demonstrates an effective phonon scattering in solid solutions with sublattice of mixed tin and lead cations. Here germanium impurity induces the dipole glass state, which is manifested in the complex dielectric susceptibility frequency dependence below 100 K.

-
- ¹ M. M. Maior, M. I. Gurzan, Sh. B. Molnar, I.P. Prits, and Yu. M. Vysochanskii, *IEEE Trans. of Ultrasonics, Ferroelectrics and Frequency Control* **47**, 877 (2000).
 - ² V. I. Litvinov, *Izv. Akad. Nauk SSSR, Ser. Fiz.* **51**, 1677 (1987).
 - ³ J. Grigas, E. Talik, K. Glukhov, K. Fedyo, I. Stoika, M. Gurzan, I. Prits, A. Grabar, and Yu. Vysochanskii, *Ferroelectrics* **418**, 134 (2001).
 - ⁴ K. Z. Rushchanskii, Yu. M. Vysochanskii, and D. Strauch, *Phys. Rev. Lett.* **99**, 207601-1 (2007).
 - ⁵ R. Yevych, V. Haborets, M. Medulych, A. Molnar, A. Kohutych, A. Dziaugys, Ju. Banys, and Yu. Vysochanskii, *Low Temp. Phys.* **42**, 1155 (2016).
 - ⁶ Yu. M. Vysochanskii, T. Janssen, R. Currat, R. Folk, J. Banys, J. Grigas, V. Samulionis, *Phase transitions in ferroelectric phosphorous chalcogenide crystals* (Vilnius University Publishing House, 2006).
 - ⁷ K. Z. Rushchanskii, R. M. Bilanych, A. A. Molnar, R. M. Yevych, A. A. Kohutych, S. I. Perechinskii, V. Samulionis, J. Banys, and Y. M. Vysochanskii, *Phys. Status Solidi B* **253**, 384 (2016).
 - ⁸ M. Blume, V. J. Emery, and R. B. Griffiths, *Phys. Rev. A* **4**, 1071 (1971).
 - ⁹ W. Hoston and A. N. Berker, *Phys. Rev. Lett.* **67**, 1027 (1991).
 - ¹⁰ Yu. M. Vysochanskii and V. Yu. Slivka, *Sov. Phys. Usp.* **35**, 123 (1992).
 - ¹¹ V. Liubachko, A. Oleaga, A. Salazar, R. Yevych, A. Kohutych, and Yu. Vysochanskii, [arXiv:1912.13398 \[cond-mat.mtrl-sci\]](https://arxiv.org/abs/1912.13398) (2019).
 - ¹² K. Moriya, K. Iwachi, M. Ushida, A. Nakagawa, K. Watanabe, S. Yano, S. Motojima, and Y. Akagi, *J. Phys. Soc. Jpn.* **64**, 1775 (1995).
 - ¹³ P. Ondrejko, M. Kempa, Y. Vysochanskii, P. Saint-Gregoire, P. Bourges, K. Rushchanskii, and J. Hlinka, *Phys. Rev. B* **86**, 224106-1 (2012).
 - ¹⁴ P. Ondrejko, M. Guennou, M. Kempa, Y. Vysochanskii, G. Garbarino, and J. Hlinka, *J. Phys.: Condens. Matter* **25**, 115901 (2013).
 - ¹⁵ K. Glukhov, K. Fedyo, J. Banys, and Yu. Vysochanskii, *Int. J. Mol. Sci.* **13**, 14356 (2012).
 - ¹⁶ V. Shvalya, A. Oleaga, A. Salazar, I. Stoika, and Yu. M. Vysochanskii, *J. Mater. Sci.* **51**, 8156 (2016).
 - ¹⁷ A. Oleaga, V. Shvalya, A. Salazar, I. Stoika, and Yu. M. Vysochanskii, *J. Alloys Compd.* **694**, 808 (2017).
 - ¹⁸ U. V. Waghmare, N. A. Spaldin, H. C. Kandpal, and Ram Seshadri, *Phys. Rev. B* **67**, 125111 (2003); A. Walsh and G. W. Watson, *J. Phys. Chem. B* **109**, 18868 (2005).
 - ¹⁹ Makoto Naka, Hitoshi Seo, and Yukitoshi Motome, *Phys. Rev. Lett.* **116**, 056402 (2016).
 - ²⁰ T. M. Rice and L. Sheddou, *Phys. Rev. Lett.* **47**, 689 (1981).
 - ²¹ R. Yevych, M. Medulych, and Yu. Vysochanskii, *Condens. Matter Phys.* **21**, 23001-1 (2018).
 - ²² I. Zamaraitė, R. Yevych, A. Dziaugys, A. Molnar, S. Svirskas, and Yu. Vysochanskii, *Phys. Rev. Appl.* **10**, 034017-1 (2018).
 - ²³ I. Zamaraitė, A. Dziaugys, Yu. Vysochanskii, and J. Banys, *Lithuanian Journal of Physics*, 2020 (in press).
 - ²⁴ Yu. Vysochanskii, K. Glukhov, M. Maior, K. Fedyo, A. Kohutych, V. Betsa, I. Prits, and M. Gurzan, *Ferroelectrics* **418**, 124 (2011).
 - ²⁵ C. L. Wang and M. L. Zhao, *J. Adv. Dielectr.* **1**, 163 (2011).
 - ²⁶ S. E. Rowley, L. J. Spalek, R. P. Smith, M. P. M. Dean, M. Itoh, J. F. Scott, G. G. Lonzarich, and S. S. Saxena, *Nature Phys.* **10**, 367 (2014).
 - ²⁷ Hideshi Fujishita, Shou Kitazawa, Masahiro Saito, Ryosuke Ishisaka, Hiroyuki Okamoto, and Toshihisa Yamaguchi, *J. Phys. Soc. Jpn.* **85**, 074703 (2016).
 - ²⁸ N. Barman, P. Singh, C. Narayana, and K. B. R. Varma, *AIP Adv.* **7**, 035105 (2017).
 - ²⁹ J. G. Bednorz and K. A. Müller, *Phys. Rev. Lett.* **52**, 2289 (1984).
 - ³⁰ Chen Ang and Zhi Yu, *Phys. Rev. B* **61**, 11363 (2000).
 - ³¹ Yu. Vysochanskii, A. Molnar, R. Yevych, K. Glukhov, and M. Medulych, *Ferroelectrics* **440**, 31 (2012).
 - ³² A. Oleaga, V. Shvalya, A. Salazar, I. Stoika, and Yu. M. Vysochanskii, *J. Alloys Compd.* **694**, 808 (2017).
 - ³³ A. Oleaga, A. Salazar, M. Massot, and Yu. M. Vysochanskii, *Termochim. Acta* **459**, 73 (2007).
 - ³⁴ A. Oleaga, A. Salazar, A. A. Kohutych, Yu. M. Vysochanskii, *J. Phys.: Condens. Matter* **23**, 025902-1 (2011).
 - ³⁵ K. Moriya, H. Kuniyoshi, K. Tashita, Y. Ozaki, S. Yano, and T. Matsuo, *J. Phys. Soc. Jpn.* **67**, 3505 (1998).
 - ³⁶ K. Moriya, T. Yamada, K. Saka, S. Yano, S. Baluya, T. Matsuo, P. Pritz, and Yu. Vysochanskii, *J. Therm. Anal. Calorim.* **70**, 321 (2002).
 - ³⁷ V. Liubachko, A. Oleaga, A. Salazar, A. Kohutych, K. Glukhov, A. Pogodin, and Yu. Vysochanskii, *Phys. Rev. Materials* **3**, 104415 (2019).
 - ³⁸ R. Folk, *Phase Transitions* **67**, 645 (1999).
 - ³⁹ Valentina Martelli, Julio Larrea Jimenez, Mucio Continentino, Elisa Baggio-Saitovitch, and Kamran Behnia, *Phys. Rev. Lett.* **120**, 125901 (2018).
 - ⁴⁰ W. H. Huber, L. M. Hernandez, and A. M. Goldman, *Phys. Rev. B* **62**, 8588 (2000).
 - ⁴¹ V. Shvalya, A. Oleaga, A. Salazar, A. Kohutych, and Yu. M. Vysochanskii, *Mater. Express* **7**, 361 (2017).
 - ⁴² P. W. Anderson, *Phys. Rev. Lett.* **34**, 953 (1975).
 - ⁴³ A. Taraphder and P. Coleman, *Phys. Rev. Lett.* **66**, 2814 (1991).
 - ⁴⁴ D. Rytz, U. T. Hchli, and H. Bilz, *Phys. Rev. B* **22**, 359 (1980).
 - ⁴⁵ S. E. Rowley, Yi-Sheng Chai, Shi-Peng Shen, Young Sun, A. T. Jones, B. E. Watts, and J. F. Scott,

- Sci. Rep. **6**, 25724 (2016).
- ⁴⁶ S. E. Rowley, M. Hadjimichael, M. N. Ali, Y. C. Durmaz, J. C. Lashley, R. J. Cava, and J. F. Scott, *J. Phys.: Condens. Matter* **27**, 395901 (2015).
- ⁴⁷ V. M. Rizak, A. A. Bokotey, I. M. Rizak, K. Al'-Shoufi, and V. Yu. Slivka, *Ferroelectrics* **192**, 149 (1997).
- ⁴⁸ S. W. H. Eijt, R. Currat, J. E. Lorenzo, P. Saint-Groire, B. Hennion, and Yu. M. Vysochanskii, *Eur. Phys. J. B* **5**, 169 (1998).